The discharge mode transition and O(5p1) production mechanism of pulsed radio frequency capacitively coupled plasma

Article *in* Applied Physics Letters · July 2012

DOI: 10.1063/1.4733662

Zilan Xiong
University of California, Berkeley
32 PUBLICATIONS **759** CITATIONS

Xinpei Lu
Huazhong University of Science and Technology
170 PUBLICATIONS **6,465** CITATIONS

AIP | Applied Physics Letters

The discharge mode transition and O(5p1) production mechanism of pulsed radio frequency capacitively coupled plasma

X. Y. Liu, J. T. Hu, J. H. Liu, Z. L. Xiong, D. W. Liu et al.

Citation: Appl. Phys. Lett. **101**, 043705 (2012); doi: 10.1063/1.4733662

View online: http://dx.doi.org/10.1063/1.4733662

View Table of Contents: http://apl.aip.org/resource/1/APPLAB/v101/i4

Published by the American Institute of Physics.

Related Articles

Surface roughness effects on the corona discharge intensity of long-term operating conductors
Appl. Phys. Lett. 101, 174103 (2012)

Experimentally investigate ionospheric depletion chemicals in artificially created ionosphere
Phys. Plasmas 19, 092901 (2012)

Account of nonlocal ionization by fast electrons in the fluid models of a direct current glow discharge
Phys. Plasmas 19, 093503 (2012)

Long range temporal correlation in the chaotic oscillations of a dc glow discharge plasma
Phys. Plasmas 19, 082313 (2012)

Numerical simulation of operation modes in atmospheric pressure uniform barrier discharge excited by a saw-tooth voltage
Phys. Plasmas 19, 083505 (2012)

Additional information on Appl. Phys. Lett.

Journal Homepage: http://apl.aip.org/

Journal Information: http://apl.aip.org/about/about_the_journal

Top downloads: http://apl.aip.org/features/most_downloaded

Information for Authors: http://apl.aip.org/authors

ADVERTISEMENT

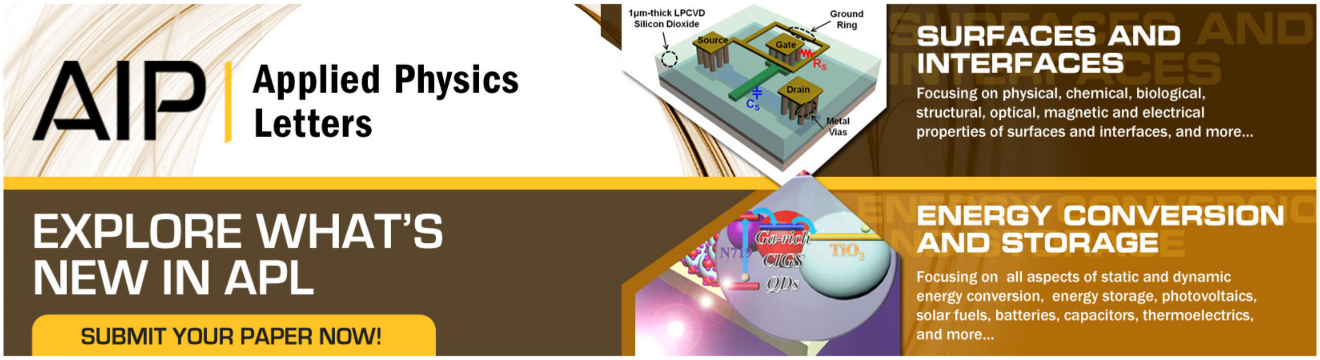

AIP | Applied Physics Letters

EXPLORE WHAT'S NEW IN APL

SUBMIT YOUR PAPER NOW!

SURFACES AND INTERFACES

Focusing on physical, chemical, biological, structural, optical, magnetic and electrical properties of surfaces and interfaces, and more...

ENERGY CONVERSION AND STORAGE

Focusing on all aspects of static and dynamic energy conversion, energy storage, photovoltaics, solar fuels, batteries, capacitors, thermoelectrics, and more...

Downloaded 19 Nov 2012 to 211.69.195.192. Redistribution subject to AIP license or copyright; see http://apl.aip.org/about/rights_and_permissions

APPLIED PHYSICS LETTERS **101**, 043705 (2012)

The discharge mode transition and O($^5p_1$) production mechanism of pulsed radio frequency capacitively coupled plasma

X. Y. Liu,[1] J. T. Hu,[1] J. H. Liu,[1] Z. L. Xiong,[1] D. W. Liu,[1,a)] X. P. Lu,[1] and J. J. Shi[2]
[1] *National State Key Lab of Advanced Electromagnetic Engineering and Technology, Huazhong University of Science and Technology, WuHan, HuBei 430074, People's Republic of China*
[2] *College of Science, Donghua University, Shanghai 201620, People's Republic of China*

(Received 13 May 2012; accepted 18 June 2012; published online 27 July 2012)

The discharge mode transition from uniform plasma across the gas gap to the α mode happens at the rising phase of the pulsed radio frequency capacitively coupled plasma (PRF CCP). This transition is attributed to the fast increasing stochastic heating at the edge of sheath. In the second stage with the stable current and voltage amplitude, the consistency between experimental and numerical spatial-temporal 777 nm emission profile suggests that He* and He_2* dominate the production of O($^5p_1$) through dissociation and excitation of O_2. Finally, the sterilization efficiency of PRF CCP is found to be higher than that of plasma jet. © *2012 American Institute of Physics*. [http://dx.doi.org/10.1063/1.4733662]

Nowadays atmospheric pressure glow discharges (APGDs) have received growing attention for many applications as nanoscience[1] and biological sterilization.[2,3] APGDs driven by kilo-Hertz sinusoid[4] and pulsed Direct Current excitations[5] are popular in biomedical applications because they can provide long plasma plume with low gas temperature. RF APGDs have been demonstrated to produce higher density of reactive species,[6–8] which is attributed to its efficient electron heating between trapped electrons and fast oscillating RF electric field.[9–11] This efficient electron heating leads to the gas temperature of hundreds degrees prevent its biomedical application, and the thermal instability of $\alpha \rightarrow \gamma$ mode transition.[9,12] Although the pulsed RF plasma has been proposed to limit the gas temperature by shorter power on duty cycle,[13–15] the discharge dynamics in the rising phase of the PRF CCP with increasing current and voltage amplitude has not been studied. On the other hand, the bactericidal effect of plasma depends on the concentration of oxidation species such as O_3, OH, and O.[3] 777 nm (O($^5p_1$) $\rightarrow$ O($^5s_2$) + $h\lambda$) emission intensity is used as an indicator of atomic oxygen concentration of plasma, but the main mechanism of O($^5p_1$) production has not been ascertained.[16] In this letter, we present experimental and numerical results aimed at elucidating the electron heating effect on mode transition from uniform plasma to α mode of the PRF CCP and the main production mechanism of O($^5p_1$). Finally, the sterilization efficiency of PRF CCP is analyzed.

The experimental setup used in this work consists of two water cooled parallel stainless steel electrodes, each being 2 cm in diameter. The discharge gap is fixed at 2 mm and the system is housed in a Perspex box. A function generator (Tektronix AFG3021B), an RF power amplifier (Ruisijieer RSG-K), and a homemade matching network are used to deliver the pulsed RF power to the power electrode. The RF frequency is 12.5 MHz and it pulse modulation frequency is 12.5 kHz. The current and the voltage across the discharge are measured with a wideband current probe (Pearson Current Monitor 2877), a wide band voltage probe (Tektronix P5100), and a digital oscilloscope (Tektronix TDS 5054B). An intensified charge-coupled device (iCCD) camera (Andor i-Star DH720) is used to take the images presented in this letter.

The plasma is simulated by 1-dimensional fluid model to get better understanding of the physics governing the discharge. The model is an extension of the one used in Refs. 9 and 17. It solves the continuity equation of each plasma specie (electron, Helium, and oxygen). The inertia of particles is neglected, and the momentum equation is substituted by the drift-diffusion approximation. Although the pulse modulation is not considered in the simulation, it still captures the discharge dynamics in the individual RF cycle and reaches good agreement with experiment data. Finally, the energy equation and continuity equation are solved self-consistently with Poisson's equation.

Fig. 1 shows the current and voltage characteristics of the PRF CCP during the power on phase. The peak applied voltage is around 640 V. The rising phase is characterized by an increasing RF oscillation amplitude for 5.7 μs. The RF voltage increased to 640 V at 3.6 μs, which was followed by

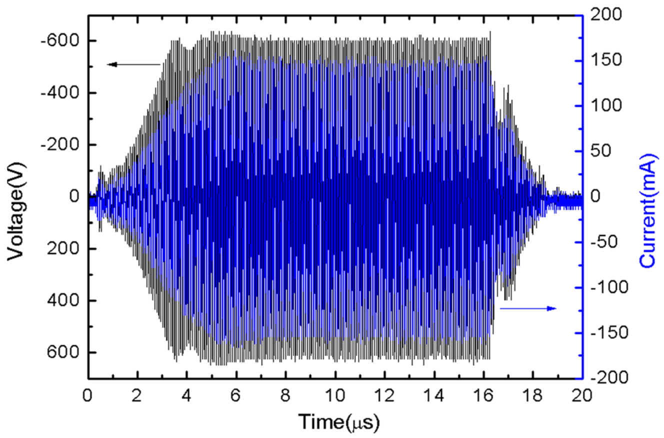

FIG. 1. Voltage and current over one power on phase.

[a)] Author to whom correspondence should be addressed. Electronic mail: liudw@hust.edu.cn.

a small valley for 0.9 μs, but the current amplitude kept increasing to 154 mA at 5.7 μs. This indicates trapped electrons and ions[11] accumulated in the gas gap and intensified the discharge until the balance between the electrons and ions production and their wall loss on electrode is matched. In the second stage, the amplitude of voltage and current was constant for 12 μs. Afterwards, the reducing voltage leads to quenching plasma in the decay period for 2 μs. Therefore the power on duty cycle is 22.5%. The gas temperature was obtained by comparing the simulated spectra of the $C^3\prod_u - B^3\prod_g(\Delta v = -2)$ band transition of nitrogen with the experiment recorded spectra.[18] Because of the water cooling, the gas temperature is 290 ± 10 K, which is 20 K less than that of the pulsed RF plasma jet.

Fig. 2 shows the space and time resolved optical emission in the rising phase during power on phase. The data shown were obtained by taking a series of 5 ns exposure time images at various RF phase, averaging emission profile in the radial direction, and collating the results to reconstruct the emission profile time evolution.[9,18] Fig. 2(a) is taken at 3.06 μs with peak RF voltage of 520 V and peak current of 90 mA. The uniform plasma bulk is across the gas gap, and its emission intensity is stronger at the voltage peak. Although the simulation cannot model all wavelength emission pattern explicitly, a good agreement is found between optical emission pattern [Fig. 2(a)] and electron generation pattern [Fig. 2(b)]. The optical emission and ionization in the plasma bulk are attributed to penetration of the applied electric field into the plasma bulk.[19] 706 nm emission is closely related to the strong electric field inside the sheath,[16,20] and the filter image at 706 nm suggests the 706 nm emission concentrated only in the region less than 0.1 mm from the cathode(data not shown). The simulation result of electric field [Fig. 2(c)] clearly shows the sheath with strong electric field around 2000 V/cm was close to the electrode within the distance ≤0.05 mm. The moderate field across the gas gap facilitates the power coupled to electrons through ohm heating, therefore, the energy deposited in the plasma bulk [Fig. 2(d)] is in the same pattern as that of optical emission observed in the experiment [Fig. 2(a)].

As the applied peak RF voltage increased to 640 V and current increased to 120 mA at 3.6 μs, besides the stronger emission from the plasma bulk, most emission concentrated near the sheath edge[9,17,21] indicates that the discharge is in the α mode [Fig. 2(e)]. The electron generation predicted by the simulation captured this transition explicitly [Fig. 2(f)], and its underestimation of the emission in the gap centre is due to the impurities (mostly N_2) not considered in the simulation. On the other hand, as the typical discharge in the α mode,[17] the 706 nm emission of this case has the same pattern as that in Fig. 3(b), and the sheath dynamics presented by the 706 nm emission pattern is also captured by the simulation result of electric field distribution shown in Fig. 2(g). Both 706 nm emission and electric field distribution suggest the maximum sheath width is 0.25 mm. The electron power density presented in Fig. 2(h) indicates that the energy coupled to the plasma is in the same pattern as that of the optical emission. The high power density region at the expanding and retreating sheath edge are attributed to the stochastic heating caused by electron interaction with fast moving plasma-sheath boundary.[22,23] The averaged stochastic heating value is $\bar{S}_{stoc} = 0.5 m_e \bar{v}_e n u_{sh}^2$ (u_{sh} is the velocity of the sheath boundary, $\bar{v}_e$ is the mean electron thermal velocity, n

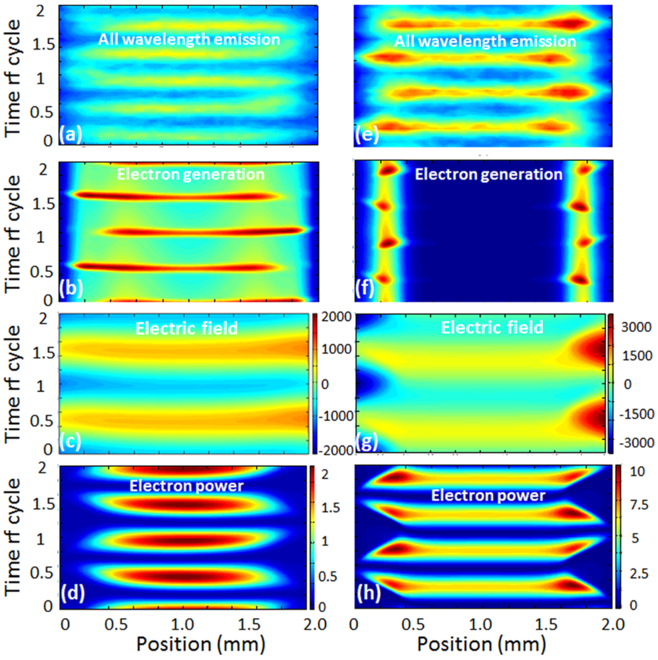

FIG. 2. (a), (e) Space- and time- resolved optical emission profiles of the discharge with (a) $I_{peak} = 90$ mA, (e) $I_{peak} = 120$ mA. (b), (f) Space- and time-resolved electron generation (numerical result). (c), (g) Space- and time-electric field (v/cm, numerical result). (d), (h) Power absorbed by the electrons calculated as J_eE (mW/cm^3) from the simulation data. Here, J_e is the electron current density and E is the electric field. (b)-(d) correspond to low current case of (a), (f), (g), and (h) correspond to high current case of (e).

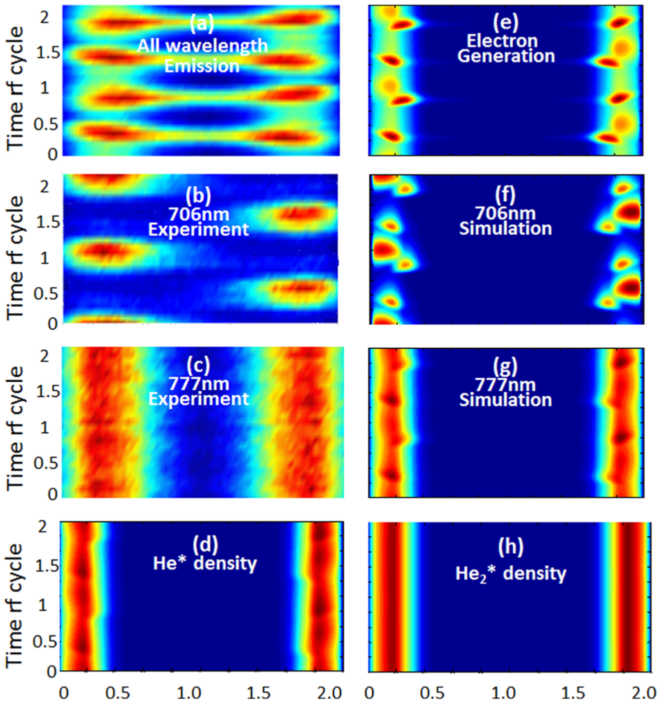

FIG. 3. Space- and time- resolved optical emission profiles (a) and numerical electron generation (e) of the discharge with $I_{peak} = 154$ mA. Space- and time- resolved optical emission at 706 nm (experiment (b) and numerical result (e)), 777 nm (experiment (c) and numerical result (g)). Space- and time-resolved density profiles of He* (d) and He2* (h) (numerical result).

is the plasma density).[23] The 5× increase of sheath leaded to 5× increase sheath velocity u_{sh} and 25× increase of stochastic heating value. As the current increased from 90 mA to 120 mA, the ohm heating in the plasma bulk $\bar{S}_{ohmb} \propto J_{rf}^2$ (Ref. 23) increased by 1.78 times. In addition to that, the omparison of averaged power density between Fig. 2(c) and 2(g) suggests that the averaged power density increased by 21 × and 2.5× at the sheath edge and gap centre, respectively, which are in agreement with the theoretical prediction above.[23] Therefore, the fast increasing stochastic heating at the boundary of enlarging sheath is the key reason for the transition from the uniform discharge to the α mode.

During the second stage, the optical emission intensity of plasma became stronger than that in the rising phase [Fig. 3(a)]. Although the working gas is helium only, due to the gas impurity and the chamber not air tight, the optical emission spectrum of RF discharge is dominated by the nitrogen species,[24] and the all wavelength emission has the same pattern as that of the 391 nm emission ($N_2^+(B^2\sum_g^+) \rightarrow N_2^+(X^2\sum_g^+) + h\lambda$), which indicates the large amount of low energy electrons ($\varepsilon > 3$ eV) to produce $N_2^+(B^2\sum_g^+)$ outside the sheath[17] as the result of stochastic heating, On the other hand, the 706 nm emission shown in Fig. 3(b) also indicates that much less high energy ($\varepsilon > 22$ eV) electrons inside the sheath.[17] Different from all wavelength emission and 706 nm emission, the 777 nm emission pattern shown in Fig. 3(c) suggests that both large amount of low energy electrons outside the sheath and the few high energy electrons inside the sheath do not affect the $O(^5p_1)$ production.

In order to study the electron heating effect on $O(^5p_1)$ production mechanism, 20 reactions between He, electron and oxygen(Table I) chosen from Refs. 16, 25, and 26 are added to the fluid model. The purity of helium used in the experiment is 99.9%. Although the gas chamber is not air tight, the helium gas is kept blowing into the chamber for 10 minutes before the experiment to insure the gas purity. Therefore, the O_2 amount in the experiment is estimated to be $\leq 0.05\%$, so the 0.05% O_2 is used in the simulation. The comparison of the all wavelength emission pattern, electron generation pattern [Figs. 3(a) and 3(e)], and experimental and numerical 706 nm emission pattern [Figs. 3(b) and 3(f)] suggested the accuracy of the simulation. The 777 nm emission obtained by simulation [Fig. 3(g)] is in the same pattern as that of the experiment [Fig. 3(c)], except a little more emission outside the sheath which might be out of resolution of the CCD camera. To help with the interpretation of Fig. 3(c), the contribution of reactions related to $O(^5p_1)$ production and consumption are compared in Fig. 4. The reaction number of Fig. 4 and Table I are the same. The dissociation and excitation of O_2 by He* and He_2* (Reactions 45 and 46) are significantly larger than electron dissociation and excitation of O_2 (Reaction 44). The spatial and temporal evolution of He* and He_2* density shown in Figs. 3(d) and 3(h) suggests that the negligible effect of the sheath on the He* and He_2* density distribution, which result in uniform 777 nm emission. The electron dissociation and excitation of O_2 (Reaction 44) contributed to the small 777 nm emission outside the sheath in the numerical result, and the contribution of ground state O excitation by electrons (Reaction 47) is negligible.

This PRF CCP provides an efficient way to decontaminate large area heat sensitive materials. In this study, its

TABLE I. Reactions between He and O_2 related with $O(^5p_1)$.

No	Reaction	Rate ($cm^{-3}s^{-1}$)	Ref.
42	$e + O_2 \rightarrow O^+ + O + 2e$	$5.3 \times 10^{-10} T_e^{0.9} \exp\left(\frac{-20}{T_e}\right)$	Ref. 24
43	$2e + O^+ \rightarrow O + e$	$5.12 \times 10^{-27} T_e^{-4.5}$	Ref. 24
44	$e + O_2 \rightarrow O(^5p1) + O + e$	$2.89 \times 10^{-10} T_e^{0.5} \exp\left(\frac{-15.9}{T_e}\right)$	Ref. 13
45	$He^* + O_2 \rightarrow O + O(^5p1) + He$	1.0×10^{-12}	Ref. 13
46	$He_2^* + O_2 \rightarrow O + O(^5p1) + 2He$	1.0×10^{-12}	Ref. 13
47	$e + O \rightarrow O(^5p1) + e$	$1.51 \times 10^{-9} T_e^{-0.45} \exp\left(\frac{-10.73}{T_e}\right)$	Ref. 13
48	$O(^5p1) \rightarrow O(^5s2) + hv$	3.69×10^{7}	Ref. 13
49	$O(^5p1) + He \rightarrow O + He$	7.0×10^{-12}	Ref. 13
50	$O(^5p1) + O_2 \rightarrow O + O_2$	1.0×10^{-9}	Ref. 13
51	$e + O \rightarrow O^+ + 2e$	$9.0 \times 10^{-9} T_e^{0.7} \exp\left(\frac{-13.6}{T_e}\right)$	Ref. 24
52	$e + O \rightarrow O^-$	1.0×10^{-15}	Ref. 23
53	$e + O + O_2 \rightarrow O^- + O_2$	1.0×10^{-31}	Ref. 23
54	$O^- + He \rightarrow He + O + e$	$2.5 \times 10^{-18} (T_g/300)^{0.6}$	Ref. 23
55	$O^- + O \rightarrow O_2 + e$	$2.0 \times 10^{-10} (T_g/300)^{0.5}$	Ref. 23
56	$O^+ + O^- \rightarrow 2O$	$2.0 \times 10^{-7} (T_g/300)^{-1}$	Ref. 23
57	$3O \rightarrow O + O_2$	$9.21 \times 10^{-34} (T_g/300)^{-0.63}$	Ref. 23
58	$2O + O_2 \rightarrow 2O_2$	$2.56 \times 10^{-34} (T_g/300)^{-0.63}$	Ref. 23
59	$He^+ + O \rightarrow O^+ + He$	$5.0 \times 10^{-11} (T_g/300)^{0.5}$	Ref. 23
60	$He_2^+ + O \rightarrow O^+ + 2He$	$1.0 \times 10^{-9} (T_g/300)^{0.5}$	Ref. 23
61	$2O + He \rightarrow He + O_2$	$1.3 \times 10^{-32} (T_g/300)^{-1} \exp\left(\frac{-170}{T_g}\right)$	Ref. 23
62	$He^* + O \rightarrow He + O^+ + e$	4.3×10^{-10}	Ref. 23

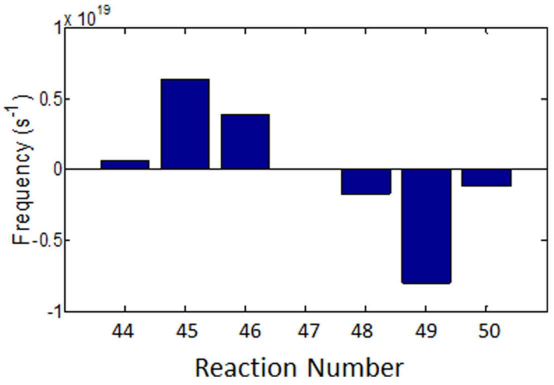

FIG. 4. Space and time averaged rate of O($^5p_1$) reaction. Positive frequency means production reactions, and negative frequency means loss reactions.

decontamination efficiency on polymers is analyzed. After an overnight incubation at 37 °C, typical S.au bacteria colonies were selected and diluted into a 10^8 cfu/ml suspension using sterile normal saline. Droplets of 100 μl of the solution were deposited on a cellulose membrane (3 cm × 3 cm) and slowly desiccated during 5 min prior to the plasma exposure. The membrane is placed on the bottom electrode and the treatment time is fixed at 10 s. After the treatment, the cellulose membrane were spread onto the surface of the LB plate and incubated for 72 h at 37 °C. Fig. 5 shows the control samples, two cases with working gas of pure helium and He + $O_2$1%, respectively. The placement of membrane did not affect the plasma structure. The treatment of ten seconds in pure helium is sufficient to decontaminate the membrane with the effective area same as electrode, furthermore, by keeping the same applied power and increasing the addition of O_2 to 1%, the decontamination area increased by 40%. This is due to the more production of O and O_3 with the addition of O_2.[27] Different from the treatment by the plasma jet, whose treatment time is in minutes scale,[28] the 10 s treatment time indicates the higher decontamination efficiency of the PRF CCP. Not only the high concentration of reactive species, but also the charged particles and the electric field between the electrode lead to the high decontamination efficiency of PRF CCP.[29]

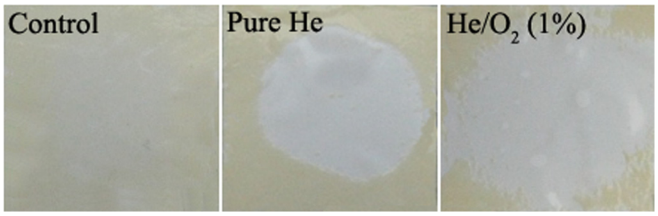

FIG. 5. Photographs of S.au samples on cellulose membrane. Plasma working time is fixed at 10 s. Working gas of pure He and He + O_2(1%) are used.

In conclusion, the transition from uniform plasma to the α mode and the production mechanism of O($^5p_1$) are studied. The fast increasing stochastic heating as the result of the expanding sheath is the key reason for this transition. He* and He_2* dominate the production of O($^5p_1$) through dissociation and excitation of O_2; therefore, the effect of sheath on 777 nm emission distribution is negligible. Reactive species, charged particles, and electric field between electrodes leaded to higher sterilization efficiency of PRF CCP than plasma jets.

This work was supported by the National Natural Science Foundation of China under Grant No. 51007029, HUST Science Foundation under Grant No. 2012QN197, and the SRF for ROCS, SEM.

[1] K. Ostrikov, J. Phys. D: Appl. Phys. **44**, 174003 (2011).
[2] D. Dobrynin, G. Fridman, G. Friedman, and A. Fridman, New J. Phys. **11**, 115020 (2009).
[3] M. G. Kong, G. Kroesen, G. Morfill, T. Nosenko, T. Shimizu, J. van Dijk, and J. L. Zimmermann, New J. Phys. **11**, 115012 (2009).
[4] M. Laroussi, IEEE Trans. Plasma Sci. **24**, 1188–1191 (1996).
[5] S. Förster, C. Mohr, and W. Viöl, Surf. Coatings Technol. **200**, 827–830 (2005).
[6] Z. Cao, Q. Nie, and M. Kong, J. Phys. D: Appl. Phys. **42**, 222003 (2009).
[7] D. B. Kim, S. Y. Moon, H. Jung, B. Gweon, and W. Choe, Phys. Plasmas **17**, 053508 (2010).
[8] Y. T. Zhang, Q. Q. Li, J. Lou, and Q. M. Li, Appl. Phys. Lett. **97**, 141504 (2010).
[9] D. W. Liu, F. Iza, and M. G. Kong, Appl. Phys. Lett. **93**, 261503 (2008).
[10] M. M. Turner and P. Chabert, Plasma Sources Sci. Technol. **16**, 364–371 (2007).
[11] D. W. Liu, J. J. Shi, and M. G. Kong, Appl. Phys. Lett. **90**, 041502 (2007).
[12] M. A. Lieberman and A. J. Lichtenberg, *Principles of Plasma Discharges and Materials Processing* (John Wiley & Sons, 2005).
[13] J. J. Shi, J. Zhang, G. Qiu, J. L. Walsh, and M. G. Kong, Appl. Phys. Lett. **93**, 041502 (2008).
[14] J. H. Liu, X. Y. Liu, K. Hu, D. W. Liu, X. P. Lu, F. Iza, and M. G. Kong, Appl. Phys. Lett. **98**, 151502 (2011).
[15] J. T. Hu, X. Y. Liu, J. H. Liu, Z. L. Xiong, D. W. Liu, X. P. Lu, F. Iza, and M. G. Kong, Phys. Plasmas **19**, 063505 (2012).
[16] J. L. Walsh, D. X. Liu, F. Iza, M. Z. Rong, and M. G. Kong, J. Phys. D: Appl. Phys. **43**, 032001 (2010).
[17] D. W. Liu, F. Iza, and M. G. Kong, Appl. Phys. Lett. **95**, 031501 (2009).
[18] J. T. Hu, X. Y. Liu, K. Hu, D. W. Liu, X. P. Lu, F. Iza, and M. G. Kong, Appl. Phys. Lett. **98**, 151502 (2011).
[19] K. McKay, F. Iza, and M. G. Kong, Eur. Phys. J. D **60**, 497–503 (2010).
[20] E. Schüngel, J. Schulze, Z. Donkó, and U. Czarnetzki, Phys. Plasmas **18**, 013503 (2011).
[21] D. Liu, F. Iza, and M. G. Kong, IEEE Trans. Plasma Sci. **36**, 952–953 (2008).
[22] V. A. Godyak and R. B. Piejak, Phys. Rev. Lett. **65**, 996–999 (1990).
[23] E. Kawamura, M. A. Lieberman, and A. J. Lichtenberg, Phys. Plasmas **13**, 053506 (2006).
[24] J. J. Shi, D. W. Liu, and M. G. Kong, Appl. Phys. Lett. **90**, 031505 (2007).
[25] D. X. Liu, P. Bruggeman, F. Iza, M. Z. Rong, and M. G. Kong, Plasma Sources Sci. Technol. **19**, 025018 (2010).
[26] D. Liu, M. Rong, X. Wang, F. Iza, M. G. Kong, and P. Bruggeman, Plasma Processes Polym. **7**, 846–865 (2010).
[27] Z. Xiong, X. P. Lu, A. Feng, Y. Pan, and K. Ostrikov, Phys. Plasmas **17**, 123502 (2010).
[28] J. Sarrette, S. Cousty, F. Clement, C. Canal, and A. Ricard, Plasma Processes Polym. **9**, 576 (2012).
[29] M. Laroussi, D. A. Mendis, and M. Rosenberg, New J. Phys. **5**, 41 (2003).